MOLECULAR SIMULATION, 2017
VOL. 43, NO. 1, 65–75
http://dx.doi.org/10.1080/08927022.2016.1233547

Taylor & Francis
Taylor & Francis Group

Effect of various surface conditions on nanochannel flows past permeable walls

Jian-Fei Xie and Bing-Yang Cao

Key Laboratory for Thermal Science and Power Engineering of Ministry of Education, Department of Engineering Mechanics, Tsinghua University, Beijing, P.R. China

ABSTRACT

In this paper, effects of surface conditions on the gas flow in nanochannels with permeable walls have been investigated by molecular dynamics simulations. The hydrodynamic characteristics of the gas flow in nanochannels, including the density distributions, slip length and boundary friction coefficient, have been significantly influenced by the molecular interactions between gas molecules and wall atoms. The density layering phenomena are observed at the fluid–wall interface under a strong fluid–wall interaction (FWI). Particularly, there is a peak of the gas density on the permeable surface where the gas density is increased and about 3 times larger than the bulk one under the strong FWI. It indicates a strong non-continuum density distribution on the permeable surface and the step down in density from nanopores to the bulk region. On the other hand, the nanoscale vortices are produced in the nanopores. Moreover, the mass flux of gas flow in nanopores is reduced, and the hydrodynamic boundary has been shifted above the permeable surface further under the weak FWI. Slip characteristics on the permeable surface under various conditions are explored. It has been found that the slip length on the permeable surface may vary as a logarithmic function with the molecular mean free path. Apparently, the skin friction on the permeable surface is affected by the velocity slip. These results are significant in the understanding of nanoscale hydrodynamics.

ARTICLE HISTORY
Received 22 February 2016
Accepted 29 August 2016

KEYWORDS
Nanochannel; permeable wall; fluid-wall interaction; molecular dynamics

1. Introduction

Nanofluidics that is inferred to the study of the behaviour, manipulation and control of fluids that are confined to structures of nanometre (typically in the length 1∼100 nm) characteristic dimensions has emerged as a discipline of science and engineering. Although transport phenomena of fluids at the nanoscale have been studied for decades, the study of nanofluidics is recently being increasingly employed. This growing interest comes from the more promising areas of nanofluidics, such as the micro/nano-electromechanical systems (MEMS/NEMS),[1–5] Lab-on-a-Chip [6–8] and micro-total-analysis systems (μTAS).[9–11] Because fluids confined in these structures of nanometre exhibit physical behaviours that are not observed in larger structures, such as those of micrometre dimensions and above, our understanding of how fluids behave at very small length scales have significant implications not only in the design of nanofluidic devices but also in the study of fundamental nanoscale science.

Usually the channel walls are assumed to be atomically smooth. Apart from the flow past the smooth solid wall, flows in channels with porous walls, named Berman flows by many authors [12,13], are used in modelling the separation of a binary mixture by gaseous diffusion, membrane separation processes,[14] filtration,[15] biological transport processes,[16] transpiration cooling and solar energy collectors. The porous wall will influence the velocity slip and slip length on the permeable surface, and in turn, the skin friction on the surface will be affected by the velocity slip. Much work has been done to investigate the effect of wall roughness on the flow in channels, including the rectangular, sinusoidal, triangular [17,18] and topological surfaces.[19] The fluid is located in the space of wall roughness where the fluid is rest and its influence on the bulk flow can be ignored.[17] The permeable surface, however, displays absolutely different pictures that the fluid can penetrate the permeable surface and flow into the nanoporous wall. In this case, the effect of the permeable surface on the hydrodynamic characteristics such as the velocity profiles and density distributions in a nanochannel must be investigated in detail.

At the nanoscale, the interfacial phenomena and fluid behaviours such as the density layering phenomena and/or slip boundary condition (SBC) are strongly influenced by the surface conditions of the solid wall, and the wall–fluid interactions have a very significant impact on the fluid flow in nanochannels. For example, Thompson and Robbins [20] and Thompson and Troian [21] changed the solid–fluid interaction energy parameter and wall density to study their effects on the slip length. Soong et al. [22] performed molecular dynamics (MD) simulations to explore the effects of wall lattice–fluid interactions on the hydrodynamic characteristics in nanochannels, and the hydrodynamics at various flow orientation angles with respect to channel walls of lattice planes (1 1 1), (1 0 0), and (1 1 0) were explored. Xie et al. [23] investigated the fluid flow in the nanochannel with a Janus interface (NCJI), especially when considering the asymmetric situations of wettability in the biology. The simulation results showed that the temperature has a significant influence on the particle number near the hydrophilic surface because the desorption increases with the fluid temperature, while the external force has a little influence on the mass distribution. Bernardi et al. [24] pointed out that the liquid properties inside nanoconfined geometries are mostly

CONTACT Bing-Yang Cao caoby@tsinghua.edu.cn

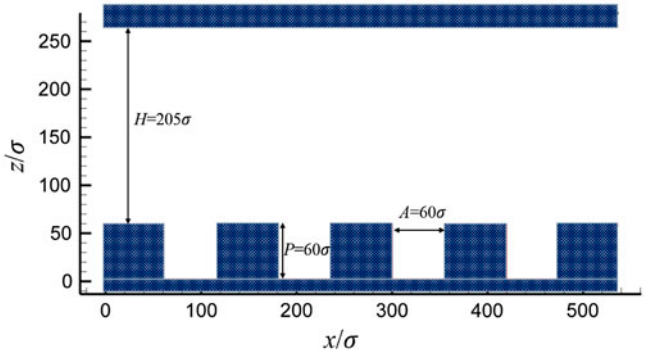

Figure 1. Geometry of a nanochannel with the permeable surface: channel length $L_x = 540\sigma$, channel height $H = 205\sigma$, and pore size $A = 60\sigma$ and $P = 60\sigma$. The y direction points into the xz plane and the channel width is $L_y = 14.3\sigma$. The upper wall is moving with a constant velocity u_0.

determined by the interactions at the interface and specifically by the wall structure which affects the first few atomic/molecular layers close to the wall surface, e.g. velocity slip. We can conclude that both the fluid structure and slip length vary widely with the commensurability in wall-fluid density and the interacting strength between wall and fluid atoms.

The effect of wall porosity on the velocity profiles and density distributions in a nanochannel has not, to the best of our knowledge, been explored previously, although much work has been devoted to the Berman flows in channels with porous walls. In addition, the hydrodynamic characteristics under various surface conditions such as the interacting strength between wall and fluid atoms have not been investigated yet, and the gas dynamics in the nanopores of the permeable walls is not well presented either. In this paper, we investigate the effect of the molecular interactions between wall and fluid atoms on the fluid flow in nanochannels with permeable walls using MD simulations, and the hydrodynamics at various surface conditions with respect to the nanoporous channel wall will be explored. The paper is organized as follows. In Section 2 the nanochannel flow is configured, the fluid-fluid and fluid-wall potential models are presented, and the SBC at nanoscales is introduced. The MD simulation results of hydrodynamic characteristics of the gas nanochannel flow under the influence of various surface conditions are presented in Section 3, including the density distributions, velocity field and the boundary friction coefficient. In Section 4 conclusions are drawn.

2. Methodology

2.1. Nanochannel flow

A three-dimensional Couette flow is considered as the flow configuration and the fluid is confined between two solid planar walls parallel to the xy plane with periodic boundary conditions imposed along the x and y axes, as shown in Figure 1. Couette flow is generated by moving the upper wall at a constant velocity u_0 along the x axis but keeping the bottom wall stationary. Each wall consists of atoms forming two planes of a face-centred-cubic (f.c.c) lattice. To maintain a well-defined solid structure with a minimum number of solid atoms, each wall atom is attached to a lattice site with a spring. A spring constant is used to control the thermal roughness of the wall and its responsiveness to the fluid. The flow is locally fully developed to be laminar with Reynolds numbers in the range of $5 \sim 50$. The simulated characteristic length, i.e. the distance between the two plates, reaches $H = 205\sigma$ which is really comparable with the characteristic size of NEMS devices in engineering situations. In the x direction, the size of the simulation cell is about $L_x = 540\sigma$ which is beyond the rough geometry in an individual computation. The permeable bottom wall is taken into account in our MD simulations, which are shown in Figure

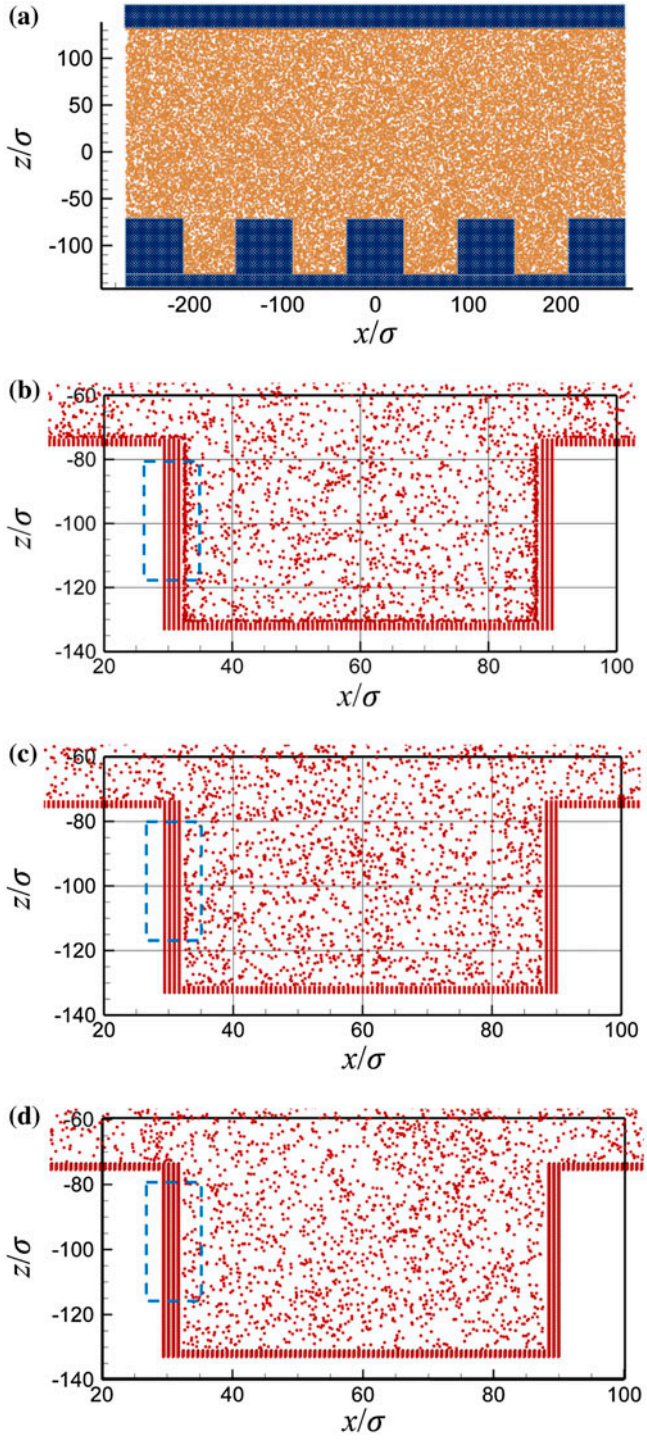

Figure 2. Nanochannel flows past the permeable surface: (a) a steady gas flow; (b) a pore-scale flow under a strong FWI ($c = 1.0$); (c) a pore-scale flow under a medium FWI ($c = 0.5$); and (d) a pore-scale flow under a weak FWI ($c = 0.25$). The directions are the same as Figure 1.

Table 1. Physical parameters in MD simulations.

Parameter	Symble	Value
Diameter	σ_A	3.405×10^{-10} m
	σ_{AP}	3.085×10^{-10} m
Energy	ε_A	1.67×10^{-21} J
	ε_{AP}	0.894×10^{-21} J
Mass	m_A	40 a.u.
	m_P	195 a.u.
Time	$\tau = \sigma_A\sqrt{m_A/\varepsilon_A}$	2.15×10^{-12} s
Temperature	ε_A/k_B	119.8 K

1, and it can be described as porosity and are characterized by an amplitude A and a space P as used in rough walls. The permeable surface is parameterized with $A = 60\sigma$ and $P = 60\sigma$. It should be pointed out that the size of the pores is much larger than the amplitude of the roughness. The magnitude of the pore size can guarantee that the gas flow in the nanochannel with the permeable surface is completely different from the one past the rough surface.

2.2. Molecular simulations

Argon-argon interactions with each other are via a Lennard-Jones (LJ) 12-6 potential in the form

$$\phi(r) = 4\varepsilon\left[\left(\frac{\sigma}{r}\right)^{12} - \left(\frac{\sigma}{r}\right)^{6}\right], \tag{1}$$

where r is the intermolecular distance, ε and σ are the energy and molecular diameter parameters, respectively. On the other hand, the argon-platinum interaction is expressed as follows

$$\phi(r)_{AP} = 4c\varepsilon_{AP}\left[\left(\frac{\sigma_{AP}}{r}\right)^{12} - \left(\frac{\sigma_{AP}}{r}\right)^{6}\right], \tag{2}$$

in which the constant c is used to control the interaction strength between the fluid molecules and wall atoms, and the larger value of c refers to a stronger fluid–wall interaction (FWI). Three magnitudes of FWI, i.e. $c = 0.25$, $c = 0.5$ and $c = 1.0$ are considered in our MD simulations, in which $c = 0.25$ refers to a weak FWI. Based on the above interactions, the physical parameters in our MD simulations are presented in Table 1. Note that all dimensional quantities such as the fluid density ρ and velocity u given by pure numbers in our MD simulations will be understood to be multiplied by an appropriate combination of σ, ε and m. For example, the moving velocity of the upper wall is set as $u_0 = 1.0\sigma_A/\tau$.

The argon molecules move according to Newton's second law and the motion equation of the ith molecule is

$$m\frac{\mathrm{d}z_i^2}{\mathrm{d}t^2} = \sum_{j\neq i}\frac{\partial\phi_{LJ}}{\partial z_i} - m\Gamma\dot{z}_i + \eta_i, \tag{3}$$

where Γ is a friction constant determining the rate of heat exchange between the simulation system and the heat reservoir, and η_i is a Gaussian distributed random force.[25] The equations of motion are integrated using a leapfrog Verlet algorithm with a time step of $\Delta t = 0.02\tau$. Particularly a typical potential cut-off of $r_{cut} = 2.5\sigma$ and the cell-linked list method are adopted to reduce the computing cost of interparticle interactions.[26] The gas and wall temperatures are both fixed at $T = 119.8$ K. The velocity rescaling technique is applied to wall atoms to maintain a constant wall temperature and the fluid system is kept at a constant temperature by a Langevin thermostat method in the z direction.[27] A typical computation in our MD simulations requires 1,000,000 time steps to reach the steady flow state. We spend about 1,500,000 additional time steps on averaging the macroscopic characteristics.

2.3. Navier boundary condition

One of the fundamental assumptions in fluid mechanical formulations of Newtonian flow past solid walls is the 'no-slip' boundary condition (NSBC): that is, the tangential component of the fluid velocity equals that of the solid on the surface. However, the microscopic origin of the no-slip condition has remained elusive for over a century. While experiments at macroscopic scales are consistent with this NSBC, recent experiments which probe molecular scales indicate that the NSBC may be different.[28]

In micro/nanoscales the SBC plays an important role in the flow development.[20,21,29–32] According to the Navier boundary condition, the slip length can be calculated by extrapolating the velocity profiles from the position in the fluid to where the velocity would vanish. Therefore, the slip length L_s can be written as

$$L_s = \frac{u_s}{\partial u/\partial z\big|_{z=0}}, \tag{4}$$

where u_s is the slip velocity, and $\partial u/\partial z$ is the local shear rate with the wall located at $z = 0$. Here we define a dimensionless slip length l_s as $l_s = L_s/H$ where H is the characteristic length of the flow geometry. Based on the SBC, Maxwell theory predicts the dimensionless slip length relevant to the Knudsen number as

$$l_s = \frac{2-\varsigma}{\varsigma}Kn, \tag{5}$$

in which ς is the tangential momentum accommodation coefficient (TMAC) defined as the fraction of gas molecules reflected diffusively from a solid surface, and Kn is the Knudsen number defined as the ratio of the molecular mean free path λ to the system characteristic length H. Maxwell theory indicates that the dimensionless slip length l_s is proportional to Kn linearly and is always positive due to the rarefaction effect.[33]

Generally the NSBC at porous walls is relaxed to account for the momentum transfer within the porous walls. When a viscous fluid flows past a porous solid, it has frequently been assumed that the tangential component of the surface velocity is zero. Although this NSBC is valid on the impermeable surface, it is not clear that it is still available on the nominal surface of a permeable material. Beavers and Joseph proposed that this NSBC is no longer valid at a permeable boundary since there is a momentum transfer resulting in a drag force that results in slip velocity at the porous interface with large open pores.[34,35] On the other hand, the fluid velocity slips on the permeable surface of porous walls such as the slip length for amorphous carbon surfaces in nanopores,[36] and it is necessary to take the SBC for the fluid flow in microporous media.[37–43] For

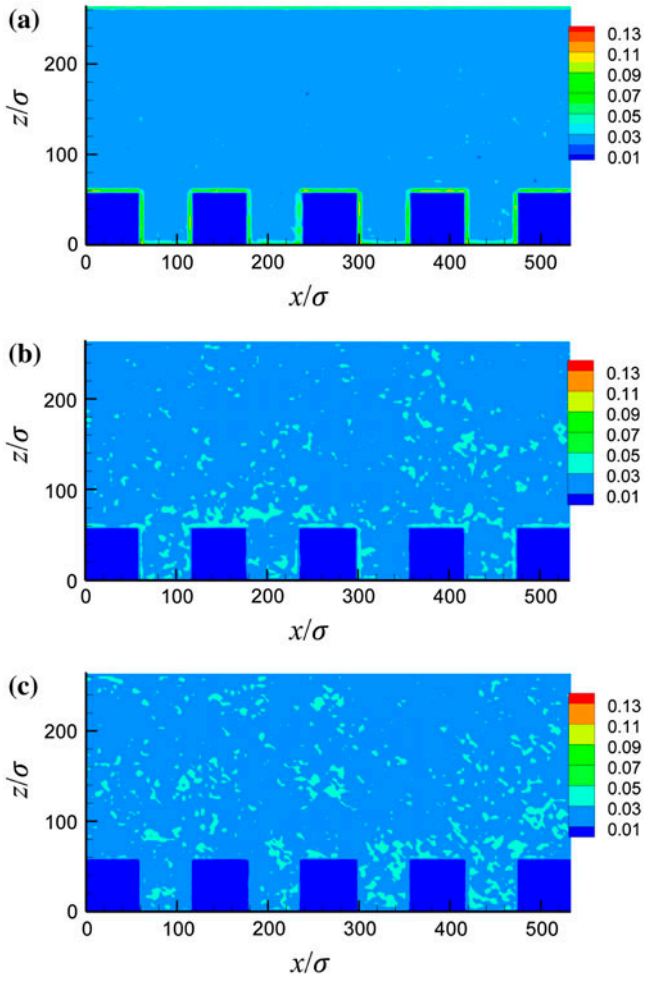

Figure 3. Density contours of the gas flow past the permeable surface: (a) under a strong FWI ($c = 1.0$); (b) under a medium FWI ($c = 0.5$); and (c) under a weak FWI ($c = 0.25$). The dark blue squares at the bottom are the solid parts of the nanochannel.

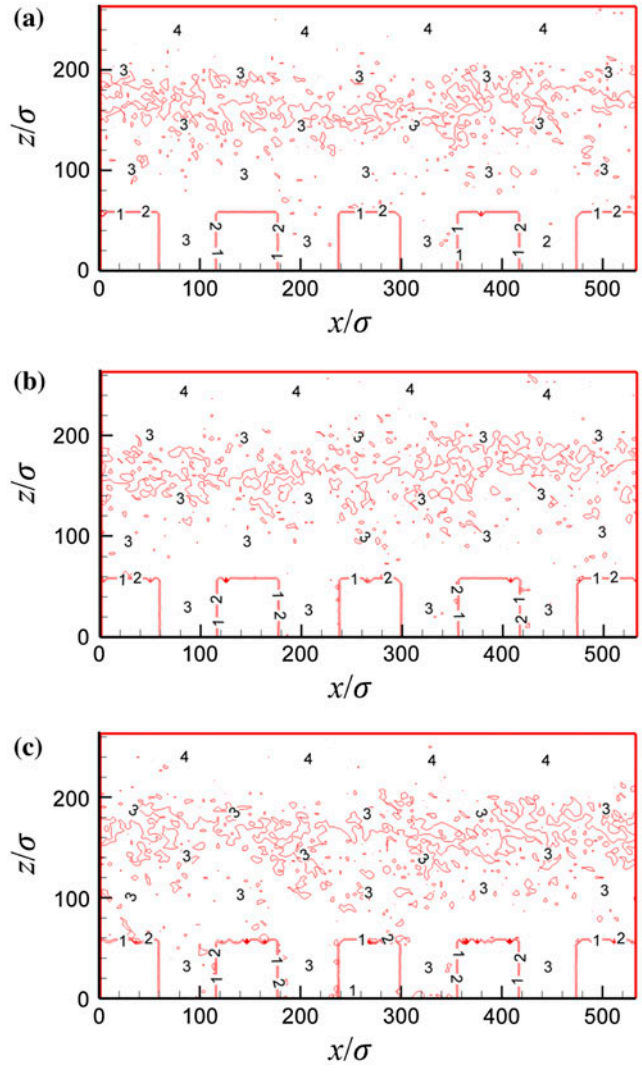

Figure 4. Pressure contours of the gas flow past the permeable surface: (a) under a strong FWI ($c = 1.0$); (b) under a medium FWI ($c = 0.5$); and (c) under a weak FWI ($c = 0.25$). The red solid lines at the bottom are the boundaries of the permeable surface.

fluid flow bounded by porous media which is permeable in the streamwise direction, many researchers have employed a slip velocity on the surface of the porous medium. For example, velocity field solutions for finite aspect ratio rectangular ducts with one porous bounding wall were obtained and employed to determine the friction factors.[44]

3. Results and discussion

3.1. Density distributions

The three-dimensional steady gas flow in the nanochannel is shown in Figure 2(a). The gas flows in the pore under the three FWI are shown in Figure 2(b)–(d). Figure 2(b) refers to the pore-scale gas flow under a strong FWI, which displays the stick of the gas molecules near the wall (indicated by a blue dotted square) and the construction of a condensed layer of gas molecules. The gas molecules are also stuck near the wall under a medium FWI, as shown in Figure 2(c), but the condensed layer of gas molecules gets thinner compared to the strong FWI. Further, there is no gas molecules that are stuck near the wall and the condensed layer disappears under a weak FWI, which is shown in Figure 2(d). We can conclude that the gas molecules can be adsorbed near the wall under the strong and medium FWI and build an ordering layer that will result in a condensed fluid density near the wall. This layering effect had been reported by Koplik et al. [29], and it was shown that the molecular ordering in the layer is the most probable location of a fluid molecule being at an f.c.c lattice site.

Density contour of the gas flow in the nanochannel is shown in Figure 3. Figure 3(a) refers to the density distribution under a strong FWI, and we find that there is a thick layer of gas molecules constructed near the wall. However, the layer of gas molecules gets thinner in the pores under a medium FWI, which is shown in Figure 3(b). Moreover, as shown in Figure 3(c), the ordering layer of gas molecules disappears completely under a weak FWI. Based on the gas equation of state, large gas density near the wall will result in a large gas pressure. The low gas density, in turn, will result in a low gas pressure near the wall. In addition, we calculate the pressure distributions in the nanochannel, which is shown in Figure 4(a)–(c). We find that there is a gas pressure gradient at the gas–wall interface under the three FWI and the gas pressure decreases gradually near the wall.

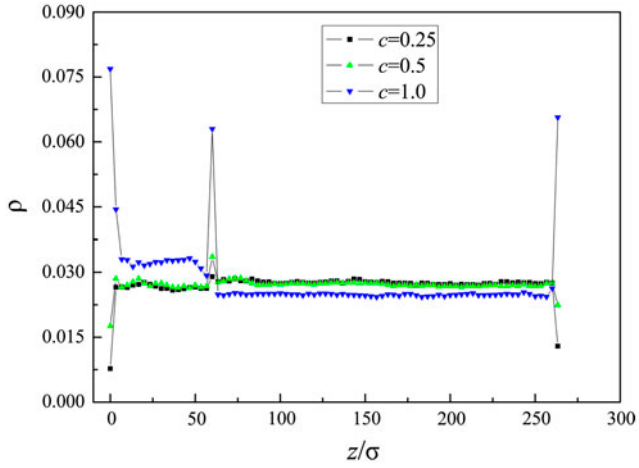

Figure 5. Density profiles of the gas flow past the permeable surface. The black squares, green triangles and blue inverted triangles represent the strong FWI ($c = 1.0$), the medium FWI ($c = 0.5$) and the weak FWI ($c = 0.25$), respectively.

We look at the density profiles of the gas molecules across the nanochannel in the z direction, i.e. along the height of the nanochannel, as shown in Figure 5. Under the strong FWI (indicated by the blue inverted triangles), the density of gas molecules near the wall is much larger than the bulk one in the main region of the nanochannel, which is consistent with the density contour observed in Figure 3(a), and the gas density in the pores is also larger than that in the main region, which is called 'step-down' in density. Particularly, there is a jump of the gas density on the permeable surface ($z = 60\sigma$) where the gas density is increased about three times larger than the bulk one. It indicates a strong non-continuum density distribution on the permeable surface. However, the density of gas molecules near the wall is much lower than the bulk one in the main region of the nanochannel under both medium and weak FWI (indicated by green triangles and black squares respectively), and the gas density in the pores is also lower than that in the main region. The condensed layer of gas molecules that results in the increase of gas density near the wall under the strong FWI cannot be built up under both medium and weak FWI. Therefore, the gas density is reduced significantly near the wall due to the weak fluid–solid bonding strengths (hydrophobic phenomena), i.e. both medium and weak FWI, and is much lower than the bulk one in the main region of the nanochannel. It can be validated in Figure 3 that the condensed layer constructed near the wall under the strong FWI contributes to the gas density increase but there is no kind of this layer under both medium and weak FWI causing the drop of gas density near the wall. In addition, the jump of the gas density on the permeable surface under both medium and weak FWI is lowered compared to the strong FWI. Recall that the gas molecules are adsorbed significantly under the strong FWI and there is a thick layer of gas molecules near the wall that is shown in Figure 3. That is the reason that there is a huge of gas molecules located in the pores resulting in a large gas density distribution. This 'trapping-desorption' behaviour is responsible for the molecular layering and oscillating density distribution near the wall.[33] Moreover, the permeable surface on the bottom wall acts as a 'swicth' that prevents the gas molecules from entering the pores. Apparently the 'swicth' results in the blockage of gas molecules on the

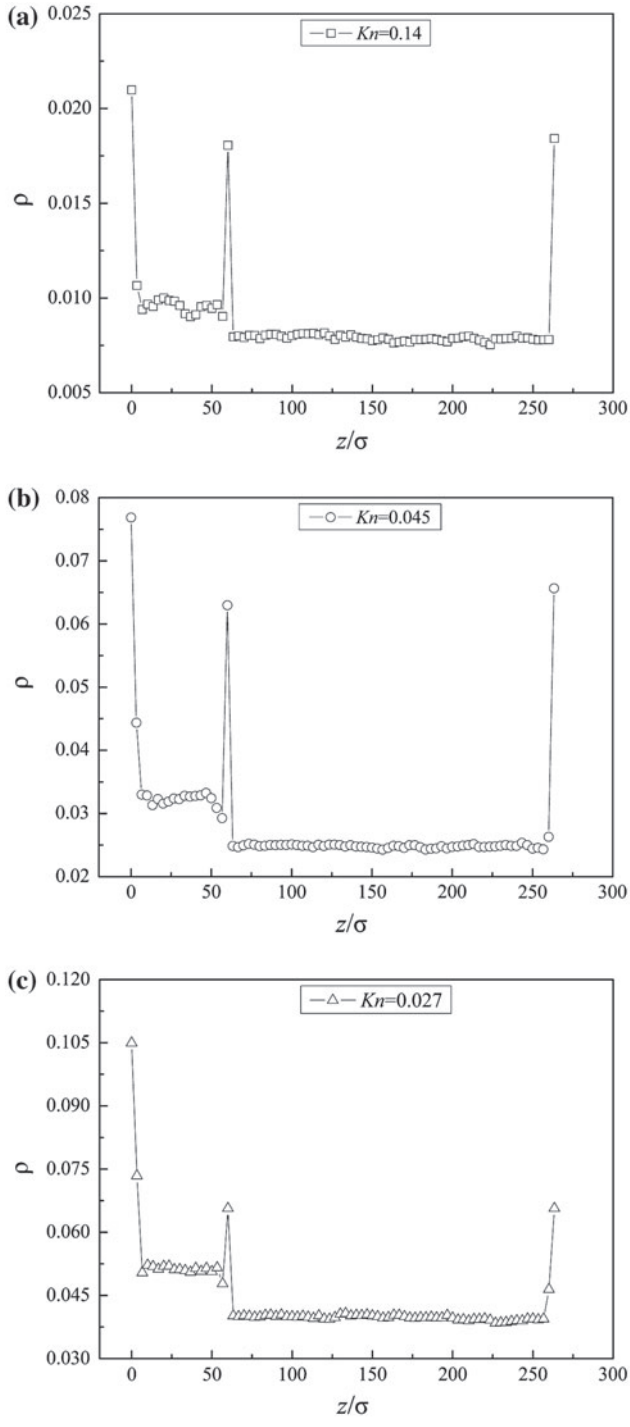

Figure 6. Density profiles of the gas flow past the permeable surface vary as a function of *Kn*: (a) $Kn = 0.14$; (b) $Kn = 0.045$; and (c) $Kn = 0.027$. The strong FWI ($c = 1.0$) is chosen here.

permeable surface and a big jump of the gas density happens under the strong FWI (indicated by the blue inverted triangles).

We further look at the jump of the gas density on the permeable surface and the effect of the rarefaction on the jump is shown in Figure 6. Figure 6(a) refers to a big jump of the gas density on the permeable surface when the rarefaction effect is strong, i.e. $Kn = 0.14$. As the rarefaction effect is reduced, i.e. $Kn = 0.045$, as shown in Figure 6(b), the jump of the gas density still exists. However, the jump is lowered significantly on the permeable surface under weaker rarefaction effect, i.e.

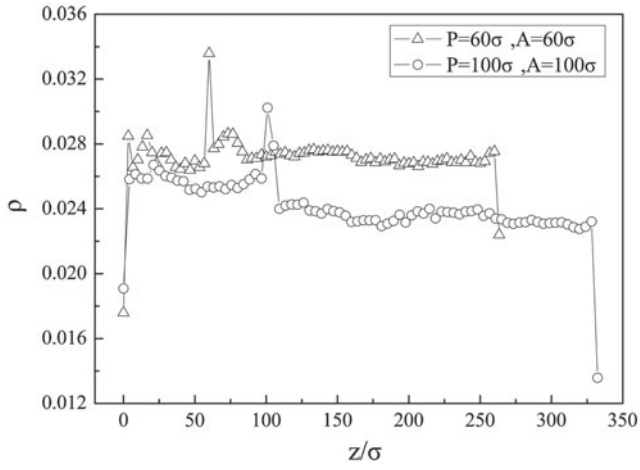

Figure 7. Influence of the pore size on density profiles of the gas flow past the permeable surfaces: triangles for pore size $A = 60\sigma$ and $P = 60\sigma$; and open circles for pore size $A = 100\sigma$ and $P = 100\sigma$. The medium FWI ($c = 0.5$) is chosen here.

$Kn = 0.027$, as shown in Figure 6(c). It can be concluded that the jump of the gas density on the permeable surface is more obvious when the rarefaction effect takes place and the jump is lowered under weaker rarefaction effect. In addition, the influence of the pore size on the gas density distribution has been investigated and is shown in Figure 7. The jump of the gas density appears on the permeable surface for both size of pores, i.e. small pore $A = 60\sigma$, $P = 60\sigma$ and large pore $A = 100\sigma$, $P = 100\sigma$, and the peak is decreased with the pore size increasing. Moreover, the gas density in the large pores is increased and larger than the bulk one compared to the small pore, which indicates that the large pores on the permeable surface are capable of capturing more gas molecules.

3.2. Velocity fields and potential energy

The interacting strength between gas and wall atoms will affect the velocity fields of the gas flow past the permeable surface, and the velocity fields of the gas flow in the nanochannel are shown in Figure 8. Under the strong FWI as shown in Figure 8(a), the gas flow produces the nanoscale vortices in the pores and the gas flow in the bulk region is influenced by the permeable surface significantly. Figure 8(b) indicates that the gas flow also produces the nanoscale vortices in the pores and the influence of the permeable surface on the gas flow in the bulk region is reduced under the medium FWI. Further, as shown in Figure 8(c), the gas flow in the bulk region is influenced by the permeable surface insignificantly and the gas flow produces few nanoscale vortices in the pores under the weak FWI compared to the strong and medium FWI. The above observation shows that the momentum transfer between gas and wall atoms is very efficient under the strong FWI.

The mass transfer between fluid and wall should be different at various surface conditions, and the mass flux ($\rho\mathbf{u}$) of the gas flow past the permeable surface of the nanochannel under the three FWI is shown in Figure 9, which indicates that the mass flux in the pores under the three FWI is all decreased. Interestingly, we find that the velocity profile of the gas flow deviates from the linear fitting indicated by the black-dotted line. As a result, the hydrodynamic boundary has been shifted

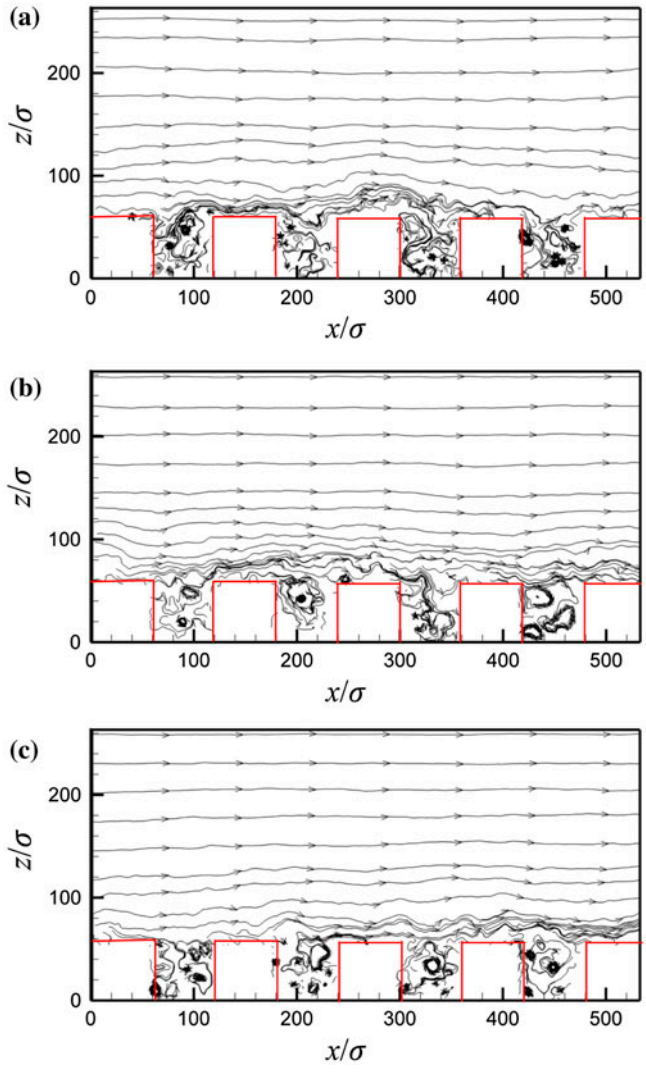

Figure 8. Velocity fields of the gas flow past the permeable surface: (a) under a strong FWI ($c = 1.0$); (b) under a medium FWI ($c = 0.5$); and (c) under a weak FWI ($c = 0.25$). The red solid lines at the bottom are the boundaries of the permeable surface.

above the permeable surface, which is indicated by the reddotted line. It means that the hydrodynamic boundary is higher than the height of pores. In addition, we find that the strength of FWI will affect the shift of the hydrodynamic boundary. Figure 9(a) refers to the strong FWI, and the hydrodynamic boundary has been shifted at $z = 90\sigma$. Figure 9(b) and (c) refer to the medium and weak FWI, and the hydrodynamic boundaries have been shifted at $z = 110\sigma$ and $z = 135\sigma$, respectively. We can conclude that the hydrodynamic boundary has been shifted more higher than the height of pores under the weak FWI.

The potential energy of the gas flow in the nanochannel is calculated and is shown in Figure 10. Under the strong FWI, as shown in Figure 10(a), the potential energy of gas molecules near the wall is large due to the adsorption of gas molecules. However, the potential energy of gas molecules near the wall is decreased under the medium and weak FWI, which are shown in Figure 10(b) and (c), respectively. It indicates that the gas molecules are stuck efficiently near the wall under the strong FWI which is responsible for the large potential energy observed

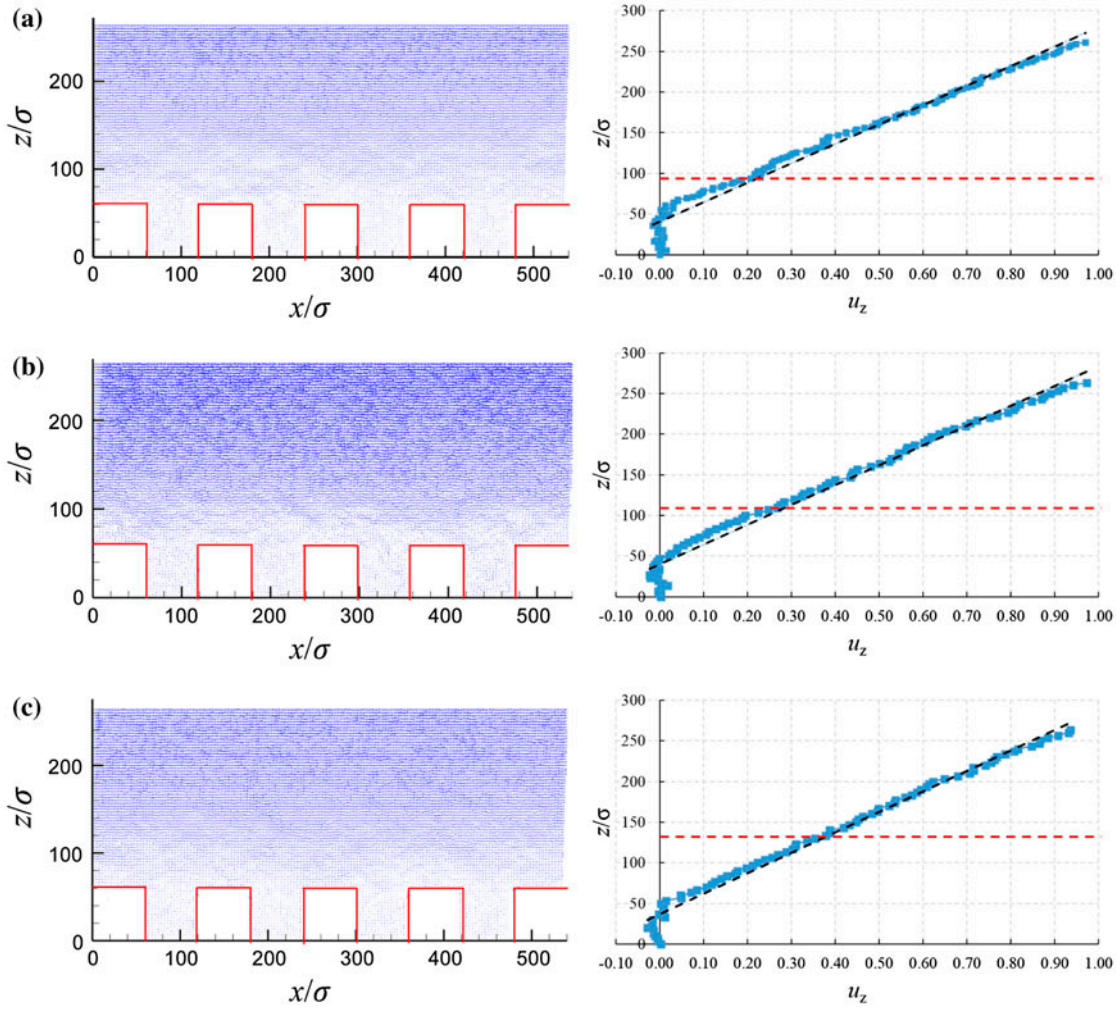

Figure 9. (Left panel) mass flux (ρv) of the gas flow past the permeable surface: (a) under a strong FWI ($c = 1.0$); (b) under a medium FWI ($c = 0.5$); and (c) under a weak FSI ($c = 0.25$). The red solid lines at the bottom are the boundaries of the permeable surface. (Right panel) velocity profiles related to the mass flux: the red-dotted lines indicate the shifted hydrodynamic boundaries, and the black-dotted lines are the fit of the velocity profiles.

near the wall. Accordingly, the kinetic energy of gas molecules has been translated to the potential energy.

3.3. Velocity profiles and slip length

We now focus on the velocity profiles of the gas flow across the nanochannel under the three FWI, which is shown in Figure 11. Figure 11(a) indicates that the velocity profiles of the gas flow are linear in the bulk region of the nanochannel. However, the velocity profiles deviate from the linear fitting and fluctuate in the pores under the three FWI. We zoom into the pore area below the permeable surface, as shown in Figure 11(b), and find that a large slip velocity u_s occurs on the permeable surface under the weak FWI resulting in a large slip length L_s. Moreover, the slip velocity on the permeable surface decreases as the FWI increasing, which refers to the reduced slip length. Therefore, the smallest slip velocity and slip length are observed under the strong FWI.

The slip length L_s that is relevant to the slip velocity can be computed using Equation (1) and is plotted as a function of Kn in Figure 12. Figure 12 indicates that the dimensionless slip l_s is an increasing function of Kn and pronounced to be a non-linear function of Kn, which is different from the prediction of Maxwell theory that the l_s is proportional to Kn linearly. In addition, the slip length is decreased as the FWI increasing, and l_s is the smallest on the permeable surface under the strong FWI. Particularly the negative slip occurs on the permeable surface under the three FWI at small Kn. That is because the layering phenomena near the wall that the nanochannel has been narrowed. On the base of the current MD simulations, the $l_s - K_n$ relationship can be well expressed by a logarithmic function

$$y = a \ln x + b, \tag{6}$$

which fits the simulation data with $a = 0.095$, 0.079 and 0.067, and $b = 0.36$, 0.28 and 0.21 for the weak, medium and strong FWI, respectively. The fitting constants a and b are decreased as the molecular interaction between gas and wall atoms increasing. It is shown that the slip length on the permeable surface may vary as a logarithmic function with the molecular mean free path. As a result, the TMAC (ς) on the permeable surface may be greater than unity due to the non-Maxwell slippage, and it is thus not limited to the range of $0 \sim 1.0$ for the permeable gas-solid condition. In addition, the influence of the pore size at the permeable surface on the slip length has been investigated and is shown in Figure 13. As the pore

size is increased from $A = 60\sigma$, $P = 60\sigma$ (open circles) to $A = 100\sigma$, $P = 100\sigma$ (open diamond), the slip length of the gas flow on the permeable surface is decreased, and it is related to Kn as a logarithmic function that is expressed by Equation (6). The fitting constants $a = 0.095, 0.067$ and $b = 0.36, 0.26$ are for the small pores and large pores, respectively, which are decreased as the pore size increasing. In order to ensure that the velocity slip has been exactly measured and the slip length has been also obtained accurately, we carry out a standard nanochannel flow past atomically smooth walls and make a comparison with both benchmark data and theoretical prediction as follows. We set up a same nanochannel of gas flow as shown in Figure 1, but the bottom wall is changed to be smooth. The MD simulations of nanochannel gas flow have been performed at different Kn, and the variation of slip length at the wall as a function of Kn is shown in Figure 14, in which benchmark data of MD and direct simulation Monte Carlo (DSMC) [30] and theoretical prediction are both shown. The theoretical prediction is based on Maxwell theory, i.e. $l_s = \alpha Kn$, in which α is the slip coefficient.[45] It can be seen in Figure 14 that the slip length obtained in our MD simulations reaches a reasonable agreement with both MD and DSMC data [30] and Maxwell theory at low Knudsen numbers ($Kn < 0.1$), but is larger than the prediction of Maxwell theory as Kn increasing. For the current MD simulations of gas nanochannel flow, $Kn \sim 0.1$, and considering an estimated relative error in mean free path of gas molecules, our MD data are in reasonable agreement with theory.

3.4. Frequency of molecules dropping into nanopores

The fluid flow on the solid wall has been well described by Maxwell theory, which assumed that the fluid molecules are diffusively reflected when they collide with the smooth solid surface. However, the fluid molecules might penetrate the surface and reside inside the wall if the surface is permeable. For example, the gas flow in the nanochannel with the permeable surface $A = 60\sigma$ and $P = 60\sigma$ is considered in present paper, and we are concerned about the molecular behaviour on the permeable wall. Our previous observations illustrate that the gas molecules travel all the time in the nanochannel even they enter the pores few times when the gas flows past the permeable surface. It is also shown that the gas flow in the pores is not rest, which is different from the fluid flow past the rough surface where the molecules are trapped and there is no flow in the rough area.[17,31] Moreover, we investigate the frequency of gas molecules entering the pores under the three FWI. Note that we colour the gas molecules that drop into the pores at the very beginning of our MD simulations and record their trajectories till the end of simulations. Then the average time of the gas molecules that entered the pores once is extracted, and each gas molecule has been tracked for 2,500,000 time steps totally. As shown in Figure 15, the distribution of gas molecules dropped into the pores of the nanochannel indicates that a large number of gas molecules enter the pore less than 10 times under the medium and weak FWI compared to the strong FWI. However, the number of gas molecules entering the pore more than 10 times is all sharply reduced under the three FWI. In addition, very few gas molecules can enter the pores

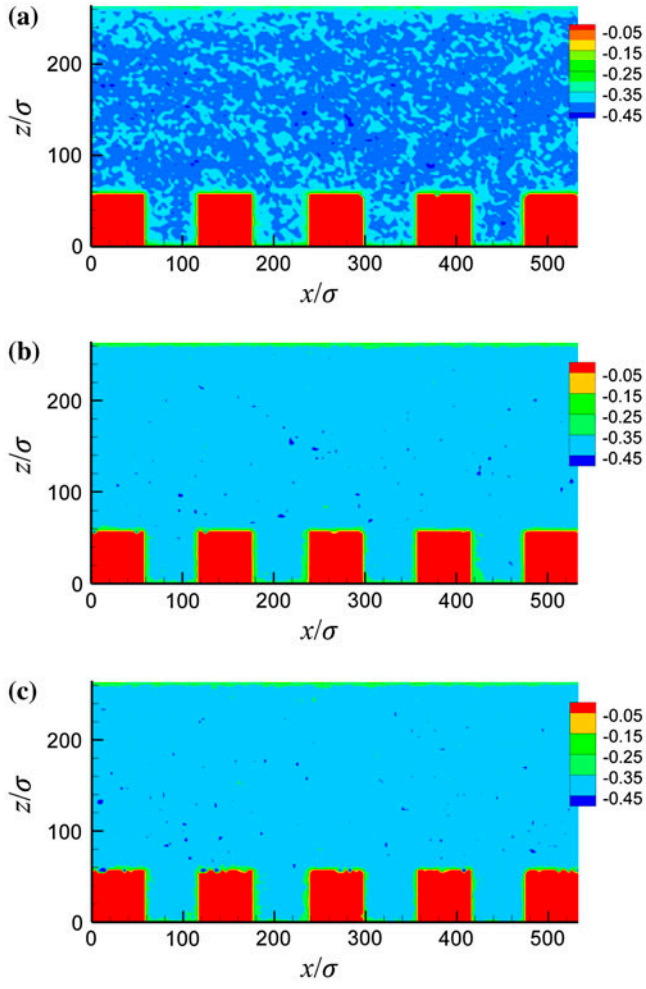

Figure 10. Potential contours of the gas flow past the permeable surface: (a) under a strong FWI ($c = 1.0$); (b) under a medium FWI ($c = 0.5$); and (c) under a weak FWI ($c = 0.25$). The red squares at the bottom are the solid parts of the nanochannel.

up to 50 times. The molecules that dropped into the pores by penetrating the permeable surface contribute to the large value of the TMAC (ς) that is greater than unity, which indicates that the diffusive reflection has been enhanced significantly on the permeable surface.

3.5. Boundary friction coefficient

The slip velocity and slippage have been influenced on the permeable surface by the molecular interaction between gas molecules and wall atoms, and in turn, the skin friction at the permeable surface is affected by the velocity slip. For the locally fully developed laminar flows in our MD simulations, the skin friction coefficient f is defined as

$$f = \frac{\tau_w}{\frac{1}{2}\rho u_0^2}, \tag{7}$$

where τ_w is the wall shear stress calculated by the net change of momentum of gas molecules at the wall per unit area and time, ρ is the gas density, and u_0 is the upper wall moving velocity as defined in Section 2. If the Maxwell slip law is applied, the normalized friction constant C^*, which represents the deviation degree of the friction coefficient from flows on the macroscale, can be theoretically expressed as

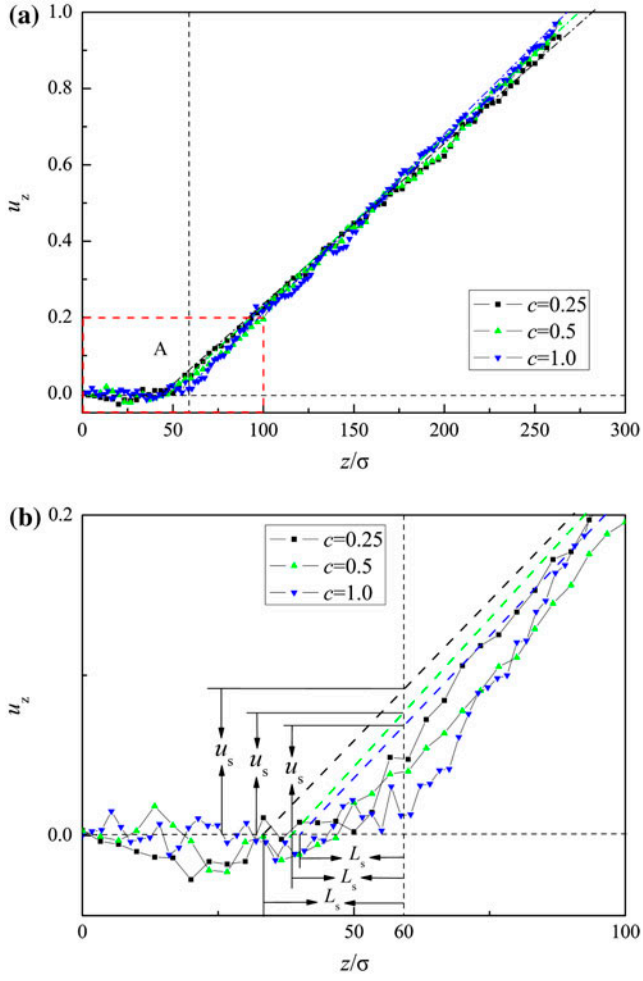

Figure 11. Velocity profiles of the gas flow past the permeable surface: (a) under a strong FWI ($c = 1.0$), under a medium FWI ($c = 0.5$) and under a weak FWI ($c = 0.25$); (b) zoom in the area of A displayed by the red-dotted square in (a). The vertical dotted line indicates the height of pores of the nanochannel. The black, green and blue diagonal dotted lines are the fit of the velocity profiles under the three FWI, respectively.

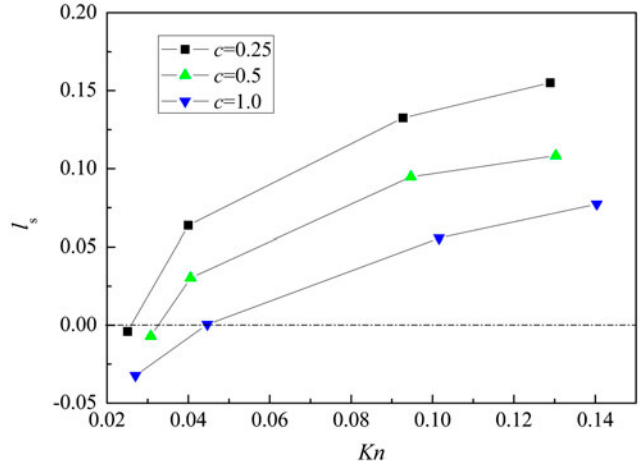

Figure 12. Slip length l_s of the gas flow past the permeable surface varies as a function of *Kn* under different FWI. The dash-dotted line refers to the NSBC.

$$C^* = \frac{1}{1 + 6\frac{2-\varsigma}{\varsigma}Kn} = \frac{1}{1 + 6l_s}. \tag{8}$$

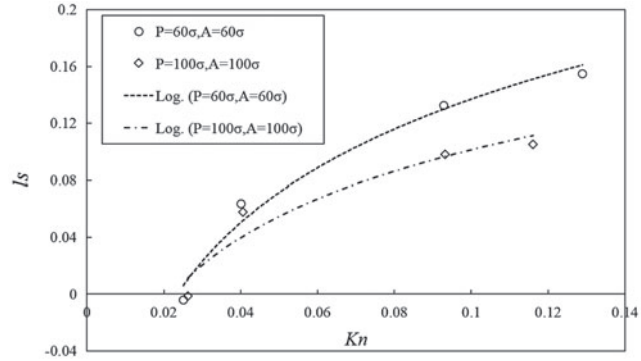

Figure 13. Influence of the pore size on the slip length l_s of gas flow past the permeable surfaces which varied as a function of *Kn*: open circles for pore size $A = 60\sigma$ and $P = 60\sigma$; and diamond for pore size $A = 100\sigma$ and $P = 100\sigma$. The dash and dash-dotted lines are the fit of the slip length for the small pores and large pores, respectively. The weak FWI ($c = 0.25$) is chosen here.

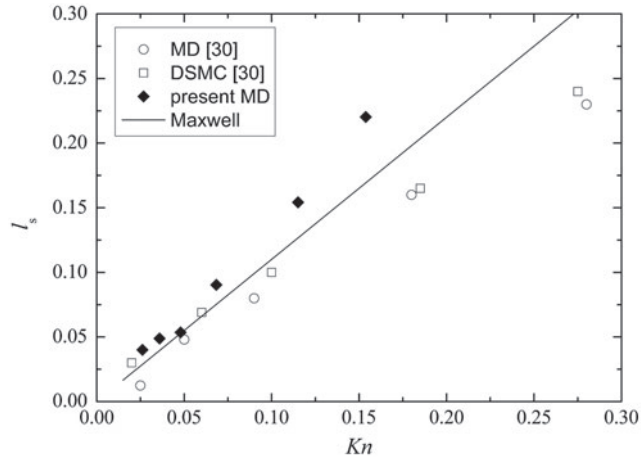

Figure 14. Slip length l_s of the gas flow past atomically smooth walls varies as a function of *Kn*. The open circles and squares refer to the MD and DSMC data of [30], and the solid line refers to Maxwell theory, respectively.

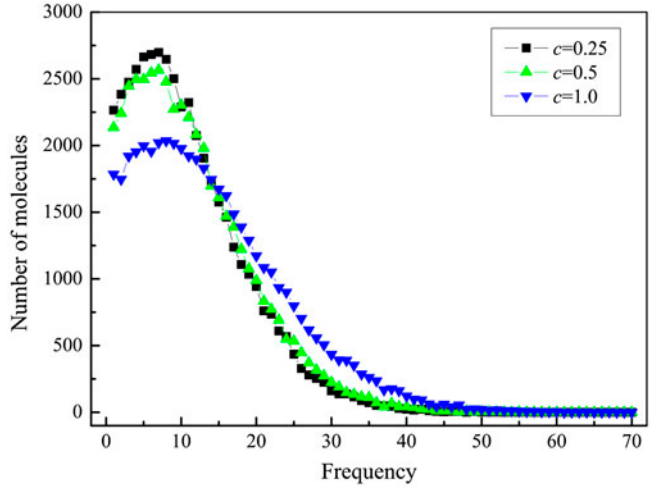

Figure 15. Distribution of gas molecules dropped into the pores of the permeable surface under the three FWI.

The friction coefficient C^* on the permeable surface as a function of *Kn* under the three FWI is plotted in Figure 16. As shown in Figure 16, the friction coefficient C^* is a decreasing function of *Kn*, and C^* on the permeable surface is increased

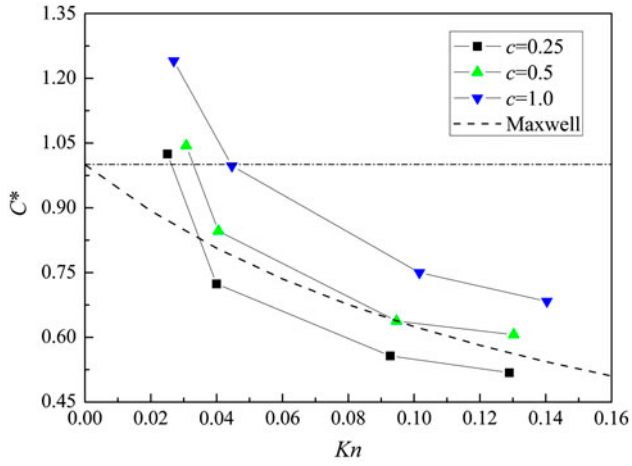

Figure 16. Friction coefficient C^* of the gas flow past the permeable surface varied as a function of *Kn* under different FWI.

with the FWI increasing. The slip length on the permeable surface is smaller under the strong FWI in the slip region, which was illustrated in Figure 12, and in turn, the smaller slip length on the permeable surface produces a larger friction coefficient in this region. It indicates that the larger friction coefficient under the strong FWI predicted in Figure 16 is consistent with the smaller slip length on the permeable surface observed in Figure 12. In addition, the friction coefficient C^* on the permeable surface under the three FWI is greater than unity (referring to the no-slip boundary and indicated by the dash-dotted line) for small $Kn(\ =\ 0.03)$, resulting from the negative slippage observed in Figure 12. The theoretical predict of the friction coefficient (indicated by the dashed line) is also shown in Figure 16 using Equation (8) with the TMAC (ς) taken equal to unity, and we find that the friction coefficient on the permeable surface under the strong and medium FWI is larger than the theoretical one if $Kn > 0.04$. It indicates that the TMAC (ς) deviates from the Maxwellian prediction due to the rarefaction effect and is out of the range of $0 \sim 1.0$. Recently Liakopoulos et al. [46] have reported a dependence of the friction factor on the geometric characteristics and quantified the associated energy dissipation of fluids moving in nanochannels. The energy dissipation consumed by the nanoscale vortices in the pores is responsible for the large friction coefficient on the permeable surface.

4. Conclusion

In this paper, effects of various surface conditions on the gas flow in nanochannels with permeable walls have been investigated by MD simulations. It is shown that the hydrodynamic characteristics of the gas flow in the nanochannel, including the density distributions, slip length and boundary friction coefficient, have been significantly influenced by the molecular interaction between gas and wall atoms. Three magnitudes of the interacting strength between gas and wall atoms have been applied in the investigations, i.e. the strong FWI, the medium FWI and the weak FWI, respectively.

The density layering phenomena were observed at the fluid–wall interface under the strong FWI and the molecular layer disappeared when the interacting strength between gas and wall atoms is weak. Particularly, there was a peak of the gas density on the permeable surface where the gas density was increased about three times larger than the bulk one under the strong FWI. It indicated a strong non-continuum density distribution on the permeable surface and the step-down in density from nanopores to the bulk region. In addition, the jump of the gas density on the permeable surface was lowered under the medium and weak interacting strength, and the blockage of gas molecules was also reduced under the weak rarefaction effect. The gas density in the large pores was increased due to its capability to capture more gas molecules.

On the other hand, the nanoscale vortices were produced in the nanopores, which influenced the bulk flow in the nanochannel. The bulk flow was affected significantly by the gas dynamics of molecules in the nanopores under the strong FWI, which indicated that the momentum transfer between gas and wall atoms was very efficient under the strong FWI. Moreover, the mass flux in nanopores was reduced under the three FWI, and the hydrodynamic boundary had been shifted above the permeable surface further under the weak interacting strength. Accordingly, the slippage on the permeable surface was affected under the three interacting strengths. It was shown that the slip length on the permeable surface may vary as a logarithmic function with the molecular mean free path and the largest slip length was decreased as the interacting strength increasing. As a result, the TMAC (ς) on the permeable surface may be greater than unity due to the non-Maxwell slippage. The slip length was decreased with the pore size increasing. Apparently, the skin friction on the permeable surface was affected by the velocity slip. The friction coefficient C^* is a decreasing function of *Kn*, and C^* on the permeable surface is increased with the FWI increasing. We can conclude that the molecular interactions between gas molecules and wall atoms have a very significant impact on the nanochannel flow characteristics, and our MD results have significant implications not only in the design of nanofluidic devices but also in the study of fundamental nanoscale science.

Acknowledgements

The financial support of National Natural Science Foundation of China and Science Fund for Creative Research Groups for this work is acknowledged. J.F.X also thanks China Postdoctoral Science Foundation for support.

Disclosure statement

No potential conflict of interest was reported by the authors.

Funding

The financial support of National Natural Science Foundation of China [grant number 51506110], [grant number 51322603]; Science Fund for Creative Research Groups [grant number 51321002]; China Postdoctoral Science Foundation [grant number 2015M581090].

References

[1] Koplik J, Banavar JR. Continuum deductions from molecular hydrodynamics. Ann Rev Fluid Mech. 1995;27:257–292.
[2] Ho CM, Tai YC. Review: MEMS and its applications for flow control. J Fluids Eng Trans ASME. 1996;118:437–447.
[3] Ho CM, Tai YC. Micro-electro-mechanical-systems (MEMS) and fluid flows. Ann Rev Fluid Mech. 1998;30:579–612.

[4] Gad-el-Hak M. The fluid mechanics of microdevices – the Freeman scholar lecture. J Fluids Eng Trans ASME. 1999;121:5–33.
[5] Cao B-Y, Sun J, Chen M, et al. Molecular momentum transport at fluid-solid interfaces in MEMS/NEMS: a review. Int J Mol Sci. 2009;10:4638–4706.
[6] Daw R, Finkelstein J. Insight: lab on a chip. Nature. 2006;442:367–418.
[7] Craighead H. Future lab-on-a-chip technologies for interrogating individual molecules. Nature. 2006;442:387–393.
[8] Bocquet L, Tabeling P. Physics and technological aspects of nanofluidics. Lab Chip. 2014;14:3143–3158.
[9] Reyes DR, Iossifidis D, Auroux P-A, et al. Micro total analysis systems. 1. Introduction, theory, and technology. Anal Chem. 2002;74:2623–2636.
[10] Kovarik ML, Ornoff DM, Melvin AT, et al. Micro total analysis systems: fundamental advances and applications in the laboratory, clinic, and field. Anal Chem. 2013;85:451–472.
[11] Culbertson CT, Mickleburgh TG, Stewart-James SA, et al. Micro total analysis systems: fundamental advances and biological applications. Anal Chem. 2014;86:95–118.
[12] Berman AS. Laminar flow in channels with porous walls. J Appl Phys. 1953;24:1232–1235.
[13] Berman AS. Concerning laminar flow in channels with porous walls. J Appl Phys. 1956;27:1557–1558.
[14] Lee C, Cottin-Bizonne C, Biance A-L, et al. Osmotic flow through fully permeable nanochannels. Phys Rev Lett. 2014;112:244501.
[15] Jensen KH, Valente AXCN, Stone HA. Flow rate through microfilters: influence of the pore size distribution, hydrodynamic interactions, wall slip, and inertia. Phys Fluids. 2014;26:052004.
[16] Ge Y, Zhu J, Kang M, et al. Ion current rectification in a confined conical nanopore with high solution concentrations. Mol Simul. 2016;121:1–6.
[17] Cao B-Y, Chen M, Guo Z-Y. Effect of surface roughness on gas flow in microchannels by molecular dynamics simulation. Int J Eng Sci. 2006;44:927–937.
[18] Cao BY. Non-Maxwell slippage induced by surface roughness for microscale gas flow: a molecular dynamics simulation. Mol Phys. 2007;105:1403–1410.
[19] Sun J, He YL, Tao WQ, et al. Multi-scale study of liquid flow in micro/nanochannels: effects of surface wettability and topology. Microfluid Nanofluid. 2012;12:991–1008.
[20] Thompson PA, Robbins MO. Shear flow near solids: epitaxial order and flow boundary conditions. Phys Rev A. 1990;41:6830–6837.
[21] Thompson PA, Troian SM. A general boundary condition for liquid flow at solid surfaces. Nature. 1997;389:360–362.
[22] Soong CY, Yen TH, Tzeng PY. Molecular dynamics simulation of nanochannel flows with effects of wall lattice-fluid interactions. Phys Rev E. 2007;76:036303.
[23] Xie H, Liu C. Molecular dynamics simulations of gas flow in nanochannel with a janus interface. AIP Adv. 2012;2:042126.
[24] Bernardia S, Searles DJ. Local response in nanopores. Mol Simul. 2015;121:1–11.
[25] Grest GS, Kremer K. Molecular dynamics simulation for polymers in the presence of a heat bath. Phys Rev A. 1986;33:3628–3631.
[26] Allen MP, Tildesley DJ. Computer simulation of liquids. Oxford: Clarendon; 1987.
[27] Thompson PA, Robbins MO. Simulations of contact line motion: slip and the dynamic contact angle. Phys Rev Lett. 1989;63:766–769.
[28] Richardson S. On the no-slip boundary condition. J. Fluid Mech. 1973;59:707–719.
[29] Koplik J, Banavar JR, Willemsen JF. Molecular dynamics of fluid flow at solid surfaces. Phys Fluids A. 1989;1:781–794.
[30] Morris DL, Hannon L, Garcia AL. Slip length in a dilute gas. Phys Rev A. 1992;46:5279–5281.
[31] Sofos FD, Karakasidis TE, Liakopoulos A. Effects of wall roughness on flow in nanochannels. Phys Rev E. 2009;79:026305.
[32] Chen Y, Zhang C, Shi M, et al. Slip boundary for fluid flow at rough solid surfaces. Appl Phys Lett. 2012;100:074102.
[33] Cao BY, Chen M, Guo ZY. Temperature dependence of the tangential momentum accommodation coefficient for gases. Appl Phys Lett. 2005;86:091905.
[34] Beavers DS, Joseph DD. Boundary conditions at a naturally permeable wall. J. Fluid Mech. 1967;30:197–207.
[35] Jeong J-T. Slip boundary condition on an idealized porous wall. Phys Fluids. 2001;13:1884–1890.
[36] Groombridgea M, Schneemilcha M, Quirkea N. Slip boundaries in nanopores. Mol Simul. 2011;37:1023–1030.
[37] Vanderlick TK, Davis HT. Self-diffusion in fluids in microporous solids. J Chem Phys. 1987;87:1791–1795.
[38] Somers SA, Davis HT. Microscopic dynamics of fluids confined between smooth and atomically structured solid surfaces. J Chem Phys. 1992;96:5389–5407.
[39] Page KS, Monson PA. Phase equilibrium in a molecular model of a fluid confined in a disordered porous material. Phys Rev E. 1996;54:R29–R32.
[40] Zhang H, Zhang BJ, Lu JW, et al. Molecular dynamics simulations on the adsorption and surface phenomena of simple fluid in porous media. Chem Phys Lett. 2002;366:24–27.
[41] Kim D, Darve E. Molecular dynamics simulation of electro-osmotic flows in rough wall nanochannels. Phys Rev E. 2006;73:051203.
[42] Hoang H, Galliero G. Local viscosity of a fluid confined in a narrow pore. Phys Rev E. 2012;86:021202.
[43] Ramon GZ, Huppert HE, Lister JR, et al. On the hydrodynamic interaction between a particle and a permeable surface. Phys Fluids. 2013;25:073103.
[44] Sparrow EM, Beavers GS, Masha BA. Laminar flow in a rectangular duct bounded by a porous wall. Phys Fluids. 1974;17:1465–1467.
[45] Xie J-F, Cao B-Y. Nanochannel flow past permeable walls via molecular dynamics. AIP Adv. 2016;6:075307.
[46] Liakopoulos A, Sofos F, Karakasidis TE. Friction factor in nanochannel flows. Microfluid Nanofluid. 2016;20:1–7.